Inorganic Chemistry

Communication

pubs.acs.org/IC

Porphyrin-Substituted H-NOX Proteins as High-Relaxivity MRI Contrast Agents

Michael B. Winter,[†,‡,∥] Piper J. Klemm,[†] Christine M. Phillips-Piro,[†,‡,#] Kenneth N. Raymond,[†] and Michael A. Marletta*[,†,‡,§,⊥,○]

[†]Department of Chemistry, [§]Department of Molecular and Cell Biology, [‡]California Institute for Quantitative Biosciences, and [⊥]Division of Physical Biosciences, Lawrence Berkeley National Laboratory, University of California, Berkeley, California 94720-3220, United States

Supporting Information

ABSTRACT: Heme proteins are exquisitely tuned to carry out diverse biological functions while employing identical heme cofactors. Although heme protein properties are often altered through modification of the protein scaffold, protein function can be greatly expanded and diversified through replacement of the native heme with an unnatural porphyrin of interest. Thus, porphyrin substitution in proteins affords new opportunities to rationally tailor heme protein chemical properties for new biological applications. Here, a highly thermally stable Heme Nitric oxide/OXygen binding (H-NOX) protein is evaluated as a magnetic resonance imaging (MRI) contrast agent. T_1 and T_2 relaxivities measured for the H-NOX protein containing its native heme are compared to the protein substituted with unnatural manganese(II/III) and gadolinium(III) porphyrins. H-NOX proteins are found to provide unique porphyrin coordination environments and have enhanced relaxivities compared to commercial small-molecule agents. Porphyrin substitution is a promising strategy to encapsulate MRI-active metals in heme protein scaffolds for future imaging applications.

Magnetic resonance imaging (MRI) has emerged as a powerful tool to profile mammalian physiology. MRI is widely used in medicine, for example, to distinguish between normal and disease tissue in patients in order to improve diagnosis and therapy. MRI has numerous advantages over other imaging strategies: it is noninvasive, able to differentiate between soft tissue, and has high lateral and depth resolution (~100 μm to ~1 mm).[1] These features allow for the construction of detailed images that provide a dynamic picture of changing physiological conditions.

MRI signal is derived from the relaxation of water molecule protons and is greatly enhanced through the implementation of contrast agents, which are currently used in 45% of MRI scans.[2] Contrast agents containing paramagnetic metals (e.g., Fe^{III}, Mn^{II}, Mn^{III}, and Gd^{III}) increase the longitudinal ($1/T_1$) and transverse ($1/T_2$) relaxation rates of nearby water molecule protons via dipole interactions.[3] A parameter termed relaxivity ($r_{n=1,2}$) is used to quantify the concentration dependence of contrast agents on proton relaxation rates (mM^{-1} s^{-1}) and can be enhanced by increasing the number of inner-sphere water molecules (q), increasing the inner-sphere water-exchange rates ($1/\tau_M$), and slowing the molecular tumbling rate ($1/\tau_R$).[4] Numerous chemical strategies have been implemented to optimize these parameters for an improved MRI signal.[5−7] In spite of the diverse frameworks developed, demetalation of contrast agents under aqueous, biological conditions has been an ongoing challenge.[8] Currently, approved contrast agents are Gd^{III}-based, but leaching of Gd^{III} has been linked to severe health problems, such as nephrogenic systemic fibrosis.[1] Additionally, Gd^{III} from hospital wastewater has been detected in the environment.[9] The high toxicity of Gd^{III} combined with increasing global demand for this rare-earth element has renewed interest in MRI contrast agents employing alternate metals and/or macromolecular scaffolds.[10−13]

To address these challenges, we have evaluated porphyrin substitution in a native heme protein scaffold as an alternative strategy to generate high-relaxivity MRI contrast agents. The Heme Nitric oxide/OXygen binding (H-NOX) domain from *Thermoanaerobacter tengcongensis* (*Tt* H-NOX) has been previously shown to be a robust platform for heme protein-based biological tools.[14,15] *Tt* H-NOX is stable under extreme temperatures (>70 °C), is highly tolerant of site-directed mutagenesis, and can be readily expressed with genetically encoded tags.[14,15] These features could be exploited to improve protein biocompatibility (e.g., through derivatization), enhance relaxivity, and facilitate targeted delivery in biology.

To evaluate *Tt* H-NOX as an MRI contrast agent, the relaxivity of the protein containing its native heme cofactor was first compared to that of myoglobin (Mb). Fe^{III} complexes display lower ionic relaxivities than lanthanides.[1,4] However, the decreased cost and lower environmental impact of Fe^{III} make it a noteworthy alternative. Relaxivities determined for high-spin, ferric aqua Mb (1.6 and 2.9 mM^{-1} s^{-1} for T_1 and T_2, respectively) were similar to previously reported values.[16] The analogous *Tt* H-NOX high-spin ferric complex[17] displayed significantly improved T_1 and T_2 relaxivities of 5.9 and 14.5 mM^{-1} s^{-1}, respectively (Figure 1 and Table 1). *Tt* H-NOX is a larger protein (22 vs 17 kDa) with a more extended conformation, which could increase the relaxivity by slowing solution tumbling. A comparison of UV−visible spectra for ferric *Tt* H-NOX and Mb (Figure 1 and Table S1 in the Supporting Information, SI) also suggests that the histidyl-ligated heme groups are in different chemical environments and/or conformations. Indeed, pre-

Received: December 6, 2012
Published: February 8, 2013

 © 2013 American Chemical Society dx.doi.org/10.1021/ic302685h | *Inorg. Chem.* 2013, 52, 2277−2279

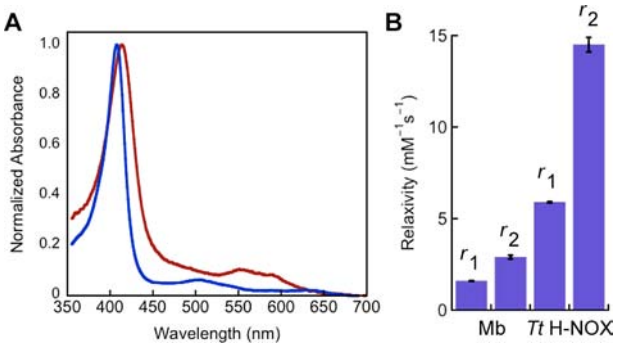

Figure 1. (A) Steady-state absorbance spectra of ferric aqua Mb (blue line) and *Tt* H-NOX (red line). (B) Relaxivities of Mb and *Tt* H-NOX at 37 °C and 60 MHz.

Table 1. Relaxivities of Protein Complexes and Select Commercial MRI Contrast Agents

complex	r_1 (mM^{-1} s^{-1})	r_2 (mM^{-1} s^{-1})	q value	ref[a]
Fe^{III} Mb	1.60 ± 0.01	2.9 ± 0.1	1	
Fe^{III} *Tt* H-NOX	5.90 ± 0.04	14.5 ± 0.4	1	
Mn^{II} *Tt* H-NOX	3.7 ± 0.1	3.8 ± 0.2	N/D	
Mn^{III} *Tt* H-NOX	12.0 ± 0.2	16.8 ± 0.5	1	
Gd^{III} *Tt* H-NOX	28.7 ± 5.0	39.9 ± 4.9	N/D	
Mn-BM3h (WT)	2.6 ± 0.1[b]	N/D	N/D	21
Mn-DPDP	2.8[c]	N/D	N/D	25
Gd-DTPA	3.3 ± 0.3	3.9 ± 0.3	1	1
Gd-DOTA	3.0 ± 0.3	3.5 ± 0.3	1	1
Gd-HP-DO3A	2.9 ± 0.3	3.4 ± 0.3	1	1

[a]This work unless noted. [b]200 MHz and 23 °C. [c]10 MHz and 25 °C. All other complexes are at 60 MHz and 37 °C. N/D = not determined.

viously published crystal structures have shown that the heme group is highly distorted in *Tt* H-NOX[18] and that the proteins have unique heme pocket architectures.[18,19] Therefore, it is possible that distinct structural features in the *Tt* H-NOX scaffold could enhance the relaxivity by modulating the heme electronic properties, increasing the inner-sphere water exchange, and/or improving the solvent accessibility to the heme pocket.

Because of the apparent higher relaxivity of the *Tt* H-NOX scaffold, its native heme cofactor was substituted with an unnatural manganese porphyrin to further improve the MRI signal. High-spin $Mn^{II/III}$ has a higher ionic relaxivity than high-spin Fe^{III}. However, small-molecule manganese complexes have seen only limited use because of aqueous demetalation.[1] Manganese(III) protoporphyrin IX was incorporated into *Tt* H-NOX (Mn^{III} *Tt* H-NOX) using an expression-based strategy employing the RP523 strain of *Escherichia coli*. The RP523 strain cannot biosynthesize heme (limiting heme contamination) and does not require heme transporter coexpression[20] unlike conventional expression hosts.[21] UV−visible spectral characterization of purified Mn *Tt* H-NOX indicated that the protein was isolated with a bound manganese(III) porphyrin (Figure 2a and Table S1 in the SI).[20] Specific manganese porphyrin substitution was confirmed by nanoelectrospray ionization (nanoESI) mass spectrometry (MS) followed by tandem MS of the intact porphyrin−protein complex (Figure S1 in the SI). Importantly, Mn^{III} *Tt* H-NOX was found to be stable under biological conditions. As with the ferric protein, Mn^{III} *Tt* H-NOX exhibited no detectible porphyrin loss or demetalation in plasma (at least 24 h at 37 °C; Figure S2 in the SI).

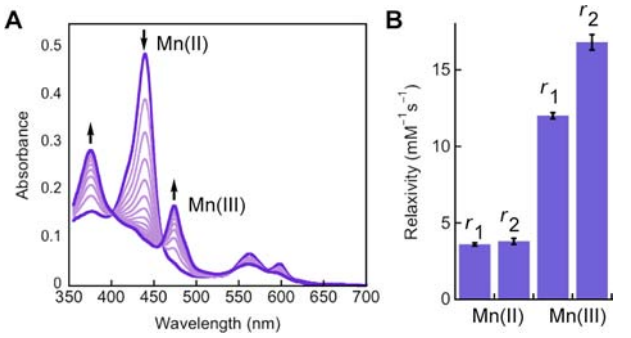

Figure 2. (A) Time-resolved UV−visible spectra of Mn^{II} to Mn^{III} *Tt* H-NOX oxidation in air at room temperature. (B) Relaxivities of Mn^{II} and Mn^{III} *Tt* H-NOX at 37 °C and 60 MHz in the absence of O_2 (Mn^{II}) and under aerobic conditions (Mn^{III}).

Both Mn^{II} and Mn^{III} *Tt* H-NOX are predicted to be paramagnetic. Therefore, T_1 and T_2 relaxivities were measured for the protein in each oxidation state. Purified Mn^{III} *Tt* H-NOX was reduced under anaerobic conditions with dithionite and found to autoxidize rapidly upon exposure to air ($t_{1/2}$ = ∼10 min at ambient temperature; Figure 2a). Therefore, the manganese(II) protein was characterized in the absence of O_2. Mn^{II} *Tt* H-NOX displayed T_1 and T_2 relaxivities of 3.6 and 3.8 mM^{-1} s^{-1}, respectively, whereas Mn^{III} *Tt* H-NOX exhibited much higher respective relaxivities of 12.0 and 16.8 mM^{-1} s^{-1} (Figure 2b and Table 1). The T_1 relaxivity of Mn^{III} *Tt* H-NOX is similar to previously described Mn-TPP derivatives.[22] However, the relaxivity is higher than that of a recently reported P450 protein substituted with manganese protoporphyrin IX (Mn-BM3h),[21] other manganese-containing proteins,[23,24] and the commercial MRI contrast agent Mn-DPDP ($S = {}^5/_2$; Table 1).[25]

To provide molecular-level insight into the high relaxivity of Mn^{III} *Tt* H-NOX, single crystals were obtained of the manganese-substituted protein under aerobic conditions. X-ray absorption spectra of the crystals collected at the Mn and Fe K-edges confirmed specific manganese incorporation and a lack of iron contamination (Figure S3 in the SI). A crystal structure of Mn^{III} *Tt* H-NOX at 2.1 Å resolution was solved by molecular replacement using the previously reported structure of heme-bound *Tt* H-NOX (PDB ID 1U55) as the search model (Figure 3 and Table S2 in the SI).[18] The crystal structure was obtained in the C_2 space group with two molecules in the asymmetric unit (herein referred to as chains A and B).

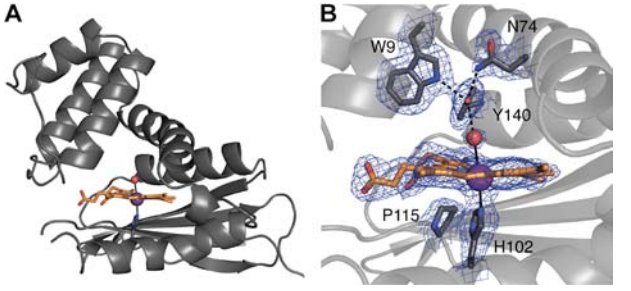

Figure 3. X-ray crystal structure of Mn^{III} *Tt* H-NOX at 2.1 Å resolution (PDB ID 4IT2). (A) Cartoon representation of monomeric Mn^{III} *Tt* H-NOX (chain B). (B) Zoom-in view of manganese(III) protoporphyrin IX bound in the heme pocket. The $2F_o - F_c$ electron density for the porphyrin, water ligand, and several heme pocket residues is shown.

dx.doi.org/10.1021/ic302685h | *Inorg. Chem.* 2013, 52, 2277−2279

The Mn *Tt* H-NOX structure was found to overlay with the heme-containing protein to a high degree overall (root-mean-square-deviation values range from 1.14 to 2.03 Å; Figure S4 in the SI). Nearly full-occupancy (>98%) porphyrin binding was also observed in the heme pocket for both protein molecules (Figure S5 in the SI). In chain B, an ordered water molecule coordinates the Mn atom and forms a hydrogen bond with a conserved distal pocket tyrosine residue (Y140; Figure 3) analogous with the iron(III) protein.[18] In addition, the conserved proximal histidine ligand (H102) binds the metal at the remaining coordination site (Figure 3). In chain A, however, the proximal histidine is in alternate bound and unbound rotamers, and no ordered water is evident at the Mn center (Figure S6 in the SI). Together, these structural data suggest greater ligand binding dynamics in Mn^{III} *Tt* H-NOX compared to the iron(III) protein. It is possible that the weakened histidine affinity in Mn^{III} *Tt* H-NOX for the oxophilic metal could open an additional water coordination site and/or improve water accessibility. Thus, built-in conformational flexibility in the *Tt* H-NOX scaffold may serve as an unanticipated mechanism to enhance agent relaxivity.

To further improve the relaxivity of *Tt* H-NOX, gadolinium(III) mesoporphyrin IX was incorporated into the protein scaffold via reconstitution of the apo protein.[26] The resulting gadolinium protein complex was found to be stable in aqueous buffer. T_1 and T_2 relaxivities recorded for Gd^{III} *Tt* H-NOX were significantly higher than those of Mn^{II}, Mn^{III}, and Fe^{III} *Tt* H-NOX. Indeed, the T_1 and T_2 relaxivities of Gd^{III} *Tt* H-NOX are ~10-fold higher than those of current commercial Gd^{III}-based agents when measured under equivalent conditions (Table 1).

Porphyrin-substituted H-NOX proteins are a promising proof-of-concept class of contrast agents for MRI technology. H-NOX scaffolds form stable metal complexes under aqueous conditions and provide unique porphyrin coordination environments. This new class of agents could be further modified through genetic or chemical means to enhance the MRI signal and biocompatibility. In addition, alternate metalloporphyrin analogues could be incorporated in the heme pocket to further improve agent properties. Together, these strategies afford new opportunities to rationally design tunable, heme protein frameworks for future biological imaging applications.

■ ASSOCIATED CONTENT

Supporting Information

Supplemental protein characterization, X-ray crystal structure data collection, and refinement statistics. This material is available free of charge via the Internet at http://pubs.acs.org.

■ AUTHOR INFORMATION

Corresponding Author

*E-mail: marletta@scripps.edu.

Present Addresses

[‖]Department of Pharmaceutical Chemistry, University of California, San Francisco, CA 94158.

[#]Department of Chemistry, Franklin & Marshall College, Lancaster, PA 17603.

[○]Department of Chemistry, The Scripps Research Institute, La Jolla, CA 92037.

Notes

The authors declare no competing financial interest.

■ ACKNOWLEDGMENTS

This work was supported by NIH Grants GM070671 (to M.A.M.) and HL069832 (to K.N.R.). We thank the QB3/Chemistry MS Facility at UC Berkeley (in particular A. Iavarone) and scientists at beamline 8.3.1 (ALS). We also thank Dr. E. S. Underbakke and Dr. A. Nierth for experimental assistance and Prof. E. E. Weinert for providing purified heme-bound *Tt* H-NOX. Finally, we thank members of the Marletta and Raymond laboratories for helpful discussions.

■ REFERENCES

(1) Port, M.; Idee, J. M.; Medina, C.; Robic, C.; Sabatou, M.; Corot, C. *Biometals* **2008**, *21*, 469−490.

(2) Ananta, J. S.; Godin, B.; Sehti, R.; Moriggi, L.; Liu, X.; Serda, R. E.; Krishnamurthy, R.; Bolskar, R. D.; Helm, L.; Ferrari, M.; Wilson, L. J.; Decuzzi, P. *Nat. Nanotechnol.* **2010**, *5*, 815−821.

(3) Klemm, P. J.; Floyd, W. C., III; Smiles, D. E.; Fréchet, J. M. J.; Raymond, K. N. *Contrast Media Mol. Imaging.* **2012**, *7*, 95−99.

(4) Laurent, S.; Forge, D.; Port, M.; Roch, A.; Robic, C.; Elst, L. V.; Muller, R. N. *Chem. Rev.* **2008**, *108*, 2064−2110.

(5) Floyd, W. C., III; Klemm, P. J.; Smiles, D. E.; Kohlgruber, A. C.; Pierre, V. C.; Mynar, J. L.; Fréchet, J. M. J.; Raymond, K. N. *J. Am. Chem. Soc.* **2011**, *133*, 2390−2393.

(6) Major, J. L.; Meade, T. J. *Acc. Chem. Res.* **2009**, *42*, 893−903.

(7) Klemm, P. J.; Floyd, W. C., III; Andolina, C. M.; Fréchet, J. M. J.; Raymond, K. N. *Eur. J. Inorg. Chem.* **2012**, *12*, 2108−2114.

(8) Nwe, K.; Bernardo, M.; Regino, C. A. S.; Williams, M.; Brechbiel, M. W. *Bioorg. Med. Chem.* **2010**, *18*, 5925−5931.

(9) Kunnemeyer, J.; Terborg, L.; Meermann, B.; Bracukmann, C.; Moller, I.; Scheffer, A.; Karst, U. *Environ. Sci. Technol.* **2009**, *43*, 2884−2890.

(10) Liepold, L. O.; Abedin, M. J.; Buckhouse, E. D.; Frank, J. A.; Young, M. J.; Douglas, T. *Nano Lett.* **2009**, *9*, 4520−6.

(11) Duncan, A. K.; Klemm, P. J.; Raymond, K. N.; Landry, C. C. *J. Am. Chem. Soc.* **2012**, *134*, 8046−9.

(12) Brustad, E. M.; Lelyveld, V. S.; Snow, C. D.; Crook, N.; Jung, S. T.; Martinez, F. M.; Scholl, T. J.; Jasanoff, A.; Arnold, F. H. *J. Mol. Biol.* **2012**, *422*, 254−262.

(13) Yang, J. J.; Yang, J.; Wei, L.; Zurkiya, O.; Yang, W.; Li, S.; Zou, J.; Zhou, Y.; Manicca, A. L. W.; Mao, H.; Zhao, F.; Malchow, R.; Zhao, S.; Johnson, J.; Hu, X.; Krogstad, E.; Liu, Z. R. *J. Am. Chem. Soc.* **2008**, *130*, 9260−9267.

(14) Boon, E. M.; Marletta, M. A. *J. Am. Chem. Soc.* **2006**, *128*, 10022−10023.

(15) Winter, M. B.; McLaurin, E. J.; Reece, S. Y.; Olea, C., Jr.; Nocera, D. G.; Marletta, M. A. *J. Am. Chem. Soc.* **2010**, *132*, 5582−5583.

(16) Modi, S.; Behere, D. V.; Mitra, S. *J. Inorg. Biochem.* **1990**, *38*, 17−25.

(17) Dai, Z.; Boon, E. M. *J. Inorg. Biochem.* **2011**, *105*, 784−792.

(18) Pellicena, P.; Karow, D. S.; Boon, E. M.; Marletta, M. A.; Kuriyan, J. *Proc. Natl. Acad. Sci. U.S.A.* **2004**, *101*, 12854−12859.

(19) Vojtechovsky, J.; Chu, K.; Berendzen, J.; Sweet, R. M.; Schlichting, I. *Biophys. J.* **1999**, *77*, 2153−2174.

(20) Woodward, J. J.; Martin, N. I.; Marletta, M. A. *Nat. Methods* **2007**, *4*, 43−45.

(21) Lelyveld, V. S.; Brustad, E.; Arnold, F. H.; Jasanoff, A. *J. Am. Chem. Soc.* **2011**, *133*, 649−51.

(22) Bryant, L. H.; Hodges, M. W.; Bryant, R. G. *Inorg. Chem.* **1999**, *38*, 1002−1005.

(23) Gupta, R. K.; Mildvan, A. S.; Schonbaum, G. R. *Arch. Biochem. Biophys.* **1980**, *202*, 1−7.

(24) Szabó, I.; Crich, S. G.; Alberti, D.; Kálmán, F. K.; Aime, S. *Chem. Commun.* **2012**, *48*, 2436−2438.

(25) Elizondo, G.; Fretz, C. J.; Stark, D. D.; Rocklage, S. M.; Quay, S. C.; Worah, D.; Tsang, Y. M.; Chen, M. C.; Ferrucci, J. T. *Radiology* **1991**, *178*, 73−78.

(26) Teale, F. W. J. *Biochim. Biophys. Acta* **1959**, *35*, 543.